

The *Escherichia coli* zinc exporter ZitB of the Cation Diffusion Facilitator (CDF) protein family: Properties, cloning, amplified expression, purification

Muhammad Ali¹, Roshan Ali¹, Israr Ali Khan¹, Irshad Ahmad¹, Nighat Nawaz² and Simon G. Patching^{3,*}

¹Institute of Basic Medical Sciences, Khyber Medical University, Peshawar 25100, Pakistan

²Department of Chemistry, Islamia College Peshawar, Peshawar 25120, Pakistan

³School of Biomedical Sciences (Astbury Building), University of Leeds, Leeds LS2 9JT, UK

*Correspondence: Professor Simon G. Patching
E-mail: s.g.patching@leeds.ac.uk, simonpatching@yahoo.co.uk

Abstract

The trace metal zinc is essential in all types of organisms, where it has many catalytic, structural and regulatory functions. Zinc homeostasis in cells and organelles is maintained by various types of zinc transport protein. These include Cation Diffusion Facilitator (CDF) family proteins, which export zinc to the extracellular space or to the cytoplasm. Homologous CDF proteins are found in both prokaryotes and eukaryotes, where the human variants are the ZnTs or SLC30 family. One of the first and best characterised prokaryotic CDFs is the *Escherichia coli* zinc exporter ZitB, which is driven by the proton motive force in an antiport manner. In this article we provide an analytical review and expand on the biochemical and computational characterisation of ZitB and assess its potential for high-resolution three-dimensional structure determination. Consistent with structures determined for other CDF proteins (YiiP, ZnTs 3, 4, 7 and 8), the 313 residues of ZitB are predicted to form six transmembrane spanning α -helices with a long cytoplasmic C-terminal tail. An unusual feature of ZitB is an exceptionally high (8.0%) content of histidine residues. Using the IPTG-inducible plasmid pTTQ18, we demonstrate the cloning and amplified expression in *E. coli* of non-tagged, wild-type ZitB at levels of ~15% of total protein in preparations of inner membranes. ZitB was solubilised in the mild detergent *n*-dodecyl- β -*D*-maltoside (DDM) and purified by immobilised metal affinity chromatography in yields of ~1.8 mg per litre of culture medium. The structural integrity of purified ZitB was confirmed by mass spectrometry and circular dichroism spectroscopy.

Key words: amino acid composition, detergent solubilisation, gene cloning, membrane protein, membrane topology, protein purification, phylogenetic analysis, zinc homeostasis

1. Introduction

The trace metal zinc is essential in all types of living things, including microorganisms, plants and animals, where it has many catalytic, structural and regulatory functions (Roohani et al., 2013; Cuajungco et al., 2021; Kiouri et al., 2023; Stiles et al., 2024). Zinc is a cofactor for many zinc-dependent proteins, and it has been estimated that 5-6% and 9-10% of proteins from prokaryotes and eukaryotes, respectively, are dependent on zinc to satisfy their biological functions (Andreini et al., 2006). In humans, zinc is essential for normal growth, development and reproduction (Frassinetti et al., 2006; Fallah et al., 2018; Brion et al., 2021; Molenda and Kolmas, 2023; Consales et al., 2024). Indeed, clinical symptoms associated with zinc deficiency include growth retardation, hypogonadism, persistent diarrhoea, alopecia, altered gastrointestinal tract function, impaired wound healing and deficient immune function (Salgueiro et al., 2000; Cuevas and Koyanagi, 2005; Kambe et al., 2015; Krebs et al., 2014; Baltaci et al., 2019). Disturbances to zinc homeostasis may contribute to or worsen various chronic diseases such as cancer, cardiovascular disease, Alzheimer's disease, diabetes and autoimmunity (Davidson et al., 2014).

The movement of zinc across biological membranes and the maintenance of zinc homeostasis in cells and organelles is enabled by zinc transporters. In humans, zinc homeostasis is maintained by 24 tissue-specific zinc transporters that comprise the ZnTs (Zn Transporters, ZnT1-10) (SLC30 family) (Palmiter and Huang, 2004; Huang and Tepasamorndech, 2013; Barber-Zucker et al., 2021) and the ZIPs (Zinc-Iron-Permeases, ZIP1-14) (SLC39 family) (Eide, 2004; Jeong and Eide, 2013), as well as metallothionein. These two transport protein families function in opposite directions to maintain zinc homeostasis. ZnTs export zinc to the extracellular space or sequester cytoplasmic zinc to intracellular compartments when zinc levels are high. ZIPs move zinc into the cytoplasm when cellular zinc levels are depleted (Kambe et al., 2015; Bin et al., 2018; Alluri et al., 2020; Hara et al., 2022; Yin et al., 2023). Malfunctions in zinc transporter expression and function have been implicated in various diseases (Baltaci and Yuce, 2018), including prostate cancer (Acevedo et al., 2024), type 1 and type 2 diabetes (Kawasaki, 2012; Davidson et al., 2014; Yi et al., 2016; Daniels et al., 2020), and bone diseases (Huang et al., 2020). Zinc transporters have roles in breast cancer progression (Takatani-Nakase, 2018) and they have been identified as therapeutic targets in Alzheimer's disease (Xu et al., 2019).

In bacteria zinc is essential for growth, survival and virulence, but high concentrations of zinc are toxic to microorganisms (Choudhury and Srivastava, 2001). Zinc homeostasis in bacteria is maintained by different types of zinc transporter. These include two zinc uptake proteins, ZnuACB and ZupT, and three families of proteins that export zinc (Suryawati, 2021). The high affinity transporter ZnuABC is a P-type ATPase that uses energy from ATP hydrolysis to drive zinc uptake. ATP hydrolysis is undertaken by ZnuC, whilst ZnuA is a soluble zinc-binding periplasmic protein that interacts with the inner membrane permease ZnuB (Patzer and Hantke, 1998; Campoy et al., 2002). ZupT is a low affinity zinc uptake protein that also imports a range of

other metals, including cadmium, iron, cobalt, copper and manganese (Grass et al., 2002; Grass et al., 2005). Zinc export is undertaken by proteins from the P-type ATPase, Resistance Nodulation Division (RND) (Routh et al., 2011; Kavanaugh et al., 2024), and Cation Diffusion Facilitator (CDF) (Haney et al., 2005; Kolaj-Robin et al., 2015) families. An example of a P-type ATPase that exports zinc from bacteria is ZntA (Rensing et al., 1997; Roberts et al., 2020; Maunders et al., 2022; Zherng et al., 2024). RND zinc export systems are comprised of three complex proteins, a cytoplasmic membrane-associated protein, a periplasmic membrane fusion protein, and an outer-membrane channel protein. An example of which is NczCBA (Valencia et al., 2013; Alav et al., 2021). Bacterial CDF zinc export proteins are secondary active transporters that are driven by the proton motive force (PMF) in an antiport manner. Examples of characterised bacterial CDF zinc exporters are CzcD (Anton et al., 1999; Martin and Giedroc, 2016; Udagedara et al., 2020), YiiP (Chao and Fu, 2004; Wei and Fu, 2006) and ZitB (Grass et al., 2001; Lee et al., 2002). Bacterial CDFs are evolutionarily most closely related to the eukaryotic ZnT/SLC30-type zinc transporters, which are also part of the CDF family (Figure 1).

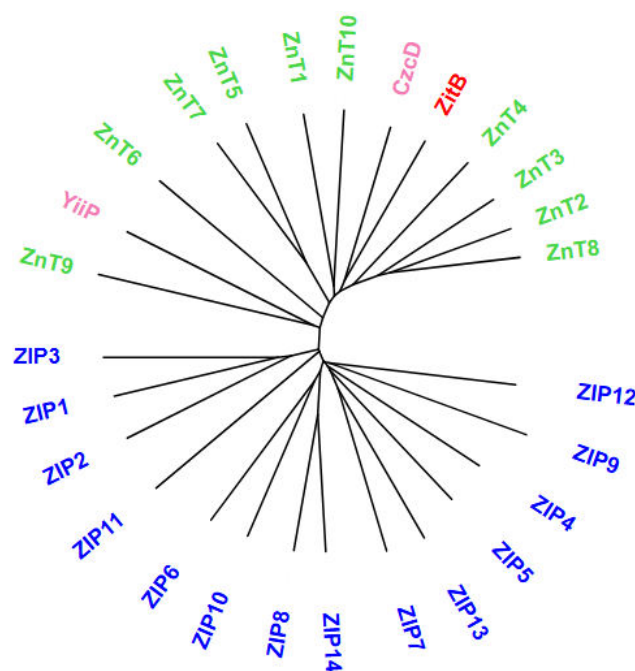


Figure 1. Evolutionary relationship of ZitB to other zinc transporters. The amino acid sequences of *E. coli* ZitB (P75757), *E. coli* YiiP (P69380), *Cupriavidus metallidurans* CzcD (P13512), human ZnTs 1-10 (Q9Y6M5, Q9BRI3, Q99726, O14863, Q8TAD4, Q6NXT4, Q8NEW0, Q8IWU4, Q6PML9 and Q6XR72, respectively) and human ZIPS 1-14 (Q9NY26, Q9NP94, Q9BRY0, Q6P5W5, Q6ZMH5, Q13433, Q92504, Q9C0K1, Q9NUM3, Q9ULF5, Q8N1S5, Q504Y0, Q96H72 and Q15043, respectively) were taken from the UniProt Knowledgebase (<https://www.uniprot.org/>) and aligned using the online tool MUSCLE (<https://www.ebi.ac.uk/jdispatcher/msa/muscle?stype=protein>) (Madeira et al., 2024). The resultant phylogenetic tree was exported in Newick format and drawn using iTOL (Interactive Tree Of Life, <https://itol.embl.de/>) (Letunic and Bork, 2007). The labels on the tree are coloured to highlight ZitB (red), YiiP and CzcD (pink), ZnTs (green) and ZIPS (blue).

The first high-resolution structures of a zinc exporter were determined by X-ray crystallography for YiiP from *Escherichia coli* in an outward-facing conformation and in complex with zinc at 3.8 Å (PDB 2QFI) (Lu and Fu, 2007) and 2.9 Å (PDB 3H90) (Lu et al., 2009). These provided a structural model for all CDF/ZnT/SLC30-type proteins (Figure 2) (Kambe et al., 2015; Kolaj-Robin et al., 2015; Cotrim et al., 2019). The overall structural organisation of YiiP is a Y-shaped homodimer with each protomer containing six transmembrane α -helices (TMHs) with both the N- and C-terminal ends at the cytoplasmic side of the membrane. The six TMHs are grouped into two bundles of four (I-II-IV-V) and two (III-VI) helices. The protein has a long (89-residues) intracellular C-terminal tail containing three C-terminal α -helices (CTH 1-3) and three C-terminal β -strands (CTS), and the intracellular loop linking TMHs IV and V is rich in histidine residues.

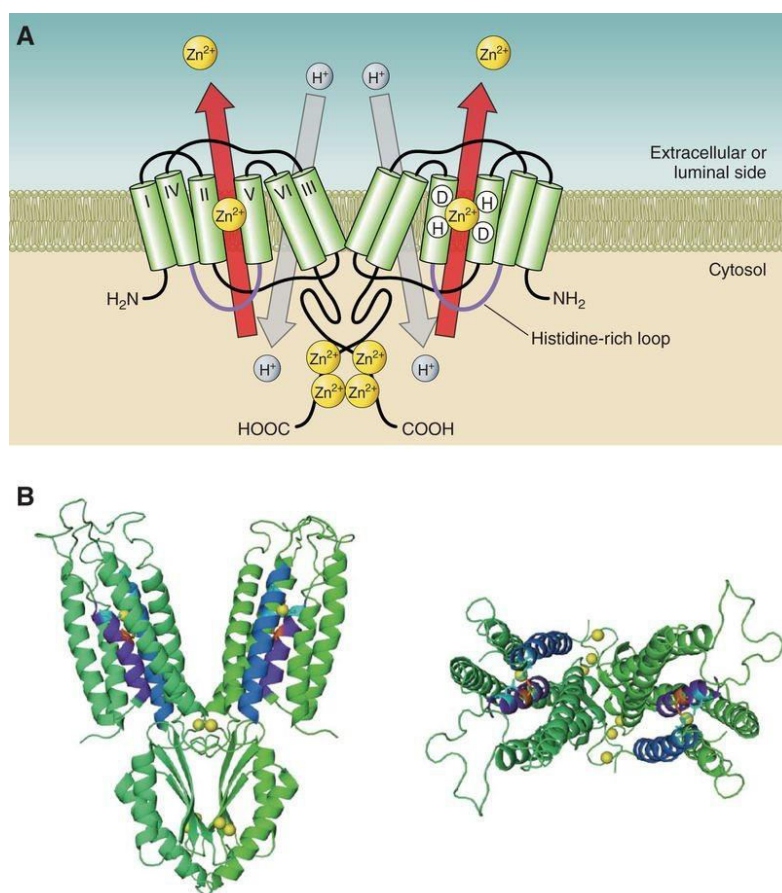


Figure 2. Structural organisation of CDF-type/ZnT/SLC30 zinc transporters. **A.** Schematic illustration of a CDF protein based on the X-ray crystal structure of the *E. coli* homolog YiiP. CDF transporters are arranged as Y-shaped dimers with six TMHs. TMHs I, II, IV, and V form a compact four-helix bundle where four conserved hydrophilic residues (HD-HD) of II and V form the intramembranous zinc-binding site. CDFs function as Zn^{2+}/H^+ exchangers, and a cytosolic histidine-rich loop is thought to be implicated in sensing and translocating zinc to the HD-HD site. **B.** Ribbon representation of the homodimeric YiiP structure (PDB 3H90). The side view (left) and top view (right) from the extracellular side are shown. Bound zinc ions in the three zinc-binding sites are represented by yellow spheres. TMHs II and V are coloured blue and purple, respectively. This figure was modified from Kambe et al. (2015).

The crystal structures of YiiP revealed three distinct zinc binding sites. Binding site A is located in the centre of the transmembrane domain and consists of four coordinating residues (D45 and D49 in TMHII, H153 and D157 in TMHV). These residues are conserved and are essential for transport activity (Wei and Fu, 2006). Binding site B is located in the cytoplasmic loop between TMHs II and III and consists of the three residues D70, H73 and H77. Binding site C is located in the C-terminal tail and consists of the five residues H234, H250, H263, H285 and D287. This site harbours four zinc ions, two from each monomer, which contribute to dimer stabilisation.

Cryoelectron microscopy (cryo-EM) structures of YiiP from *Shewanella oneidensis* were later determined at resolutions of 4.1 Å (PDB 5VRF) and 4.0 Å (PDB 7KZX) in an inward-facing conformation and in complex with zinc (Lopez-Redondo et al., 2018; Hussein et al., 2023). Since then, cryo-EM structures have been determined for ZnT3, ZnT4, ZnT7 and ZnT8 from *Homo sapiens* (Xue et al., 2020; Bui et al., 2023; Ishida et al., 2025) and ZnT8 from *Xenopus tropicalis* (Zhang et al., 2023) (Table 1). Whilst these structures have provided insights into the molecular mechanisms of CDF proteins, elucidation of further structures would enable a more comprehensive understanding about how they function and potentially provide information for CDF proteins to serve as therapeutic targets.

A major bottleneck to overcome for high-resolution structure determination of membrane proteins is to achieve amplified expression and to produce sufficient quantities of purified protein as close as possible to their native membrane environment (Poolman and Knol, 1999; Ward et al., 1999; Ahmad et al., 2018). In a topology-informed strategy for amplifying the expression of variously tagged bacterial membrane proteins, ZitB from *E. coli* was one of the proteins used to demonstrate the approach (Rahman et al., 2007). A high-resolution structure of ZitB is not yet available, so in this article we will focus on what is known about ZitB so far and assess its potential for further structure-function studies.

2. Materials and Methods

2.1. Computational methods

Protein sequences were taken from the UniProt Knowledgebase (<https://www.uniprot.org/>). Membrane protein topology was predicted using the online tools DeepTMHMM (<https://dtu.biolib.com/DeepTMHMM>) (Hallgren et al., 2022) and TOPCONS (<https://topcons.cbr.su.se/>) (Tsirigos et al., 2015). The amino acid compositions of proteins were calculated using the online ExPASy tool ProtParam (<https://web.expasy.org/protparam/>) (Gasteiger et al., 2005). Protein sequences were aligned using the online tool MUSCLE (<https://www.ebi.ac.uk/jdispatcher/msa/muscle?stype=protein>) (Madeira et al., 2024). For phylogenetic analysis, protein sequences were aligned using MUSCLE, then the resultant phylogenetic tree was exported in Newick format and drawn using iTOL (Interactive Tree Of Life, <https://itol.embl.de/>) (Letunic and Bork, 2007).

Protein / Organism	Oligomeric state / Conformation	Ligand state	Method / Resolution	PDB entry	Reference
YiiP / <i>Escherichia coli</i>	Homodimer / Outward-facing	Zn ²⁺	X-ray/3.8 Å X-ray/2.9 Å	2QFI 3H90	Lu & Fu, 2007 Lu et al., 2009
YiiP / <i>Shewanella oneidensis</i>	Homodimer / Inward-facing	Zn ²⁺	EM/4.1 Å	5VRF	Lopez-Redondo et al.,
	Homodimer / Inward-facing occluded	Zn ²⁺	EM/4.0 Å	7KZX	Hussein et al., 2023
ZnT3 / <i>Homo sapiens</i>	Homodimer / Inward-facing	Zn ²⁺	EM/3.14 Å	8XN1	Ishida et al., 2025
ZnT4 / <i>Homo sapiens</i>	Homodimer / Outward-facing		EM/3.0 Å		Ishida et al., 2025
ZnT7 / <i>Homo sapiens</i>	Homodimer / Outward-facing	Apo	EM/2.2 Å	8J7T	Bui et al., 2023
	Homodimer / Outward-facing	Zn ²⁺	EM/3.12 Å	8J7U	
	Heterodimer / Inward + Outward-facing	Apo	EM/2.79 Å	8J7V	
	Heterodimer / Inward + Outward-facing	Zn ²⁺ , Apo	EM/2.68 Å	8J80	
	Heterodimer / Inward + Outward-facing	Zn ²⁺	EM/2.92 Å	8J7W	
ZnT8 / <i>Homo sapiens</i>	Homodimer / Outward-facing	Zn ²⁺	EM/4.1 Å	6XPE	Xue et al., 2020
	Heterodimer / Inward + Outward-facing	Apo	EM/5.9 Å	6XPF	
ZnT8 / <i>Xenopus tropicalis</i>	Homodimer / Outward-facing	Zn ²⁺	EM/3.85 Å	7Y5G	Zhang et al., 2023
	Homodimer / Outward-facing	Apo	EM/3.72 Å	7Y5H	

Table 1. High-resolution structures of CDF family proteins.

2.2. Laboratory methods

2.2.1. Isolation of plasmid DNA

E. coli cells harbouring the relevant plasmid were grown overnight in Luria-Bertani (LB) liquid medium (5 mL) in 50 mL Falcon tubes at 37 °C in an orbital incubator at 200 rpm and collected by centrifugation (2,200 x g, 4 °C, 10 min). Plasmid DNA was isolated from the cells using a QIAprep Spin Miniprep Kit (Qiagen Ltd, Crawley, West Sussex, UK) following the manufacturer's instructions and then stored at -20 °C.

2.2.2. Electrophoretic separation of DNA on an agarose gel and estimation of size and concentration

Agarose gel electrophoresis (Sambrook et al., 1989) was performed using a Sub-Cell Model 96 apparatus (Bio-Rad, Hercules, California, USA) with Tris-acetate-EDTA (TAE) buffer and gels were stained using SYBR Safe™ dye (Invitrogen, Waltham, Massachusetts, USA). DNA samples and marker DNA were mixed with 5x DNA

sample buffer [50% glycerol, 50 mM EDTA (pH 8.0) and 0.05% bromophenol blue] before loading on to the gel. Electrophoresis was performed at constant voltage at 80-90 V for ~30 min to 1 h and then visualised by illumination under blue light. The amount of DNA in samples was estimated by comparing its intensity with that of known amounts of marker DNA (1 Kb DNA marker) (New England Biolabs, Ipswich, Massachusetts, USA).

2.2.3. Polymerase chain reaction (PCR)

PCR was conducted according to the manufacturer of KOD Hot Start DNA polymerase (Novagen, Lagos, Nigeria). A typical PCR mixture had the following components: 5 μ L of 10x PCR buffer for KOD Hot Start DNA polymerase, 1 μ L each of forward and reverse primers (10 pmol/ μ L each primer, final concentration 0.6 μ M), 5 μ L of 2 mM dNTPs (final concentration 0.2 mM), 3 μ L of 25 mM MgSO₄ (final concentration 1.5 mM), 1 μ L of template DNA (50-100 ng), 2 μ L of KOD Hot Start DNA polymerase (1 U/ μ L), 33 μ L Milli-Q[®] filter sterilized water. The samples were centrifuged briefly to bring the reaction components to the bottom of the tube. Amplification was performed using a 'Touchdown' PCR approach (Don et al. 1991). Samples were loaded on to a VWR[®] UNO96 thermal cycler (West Chester, Pennsylvania, USA) equipped with a 96-well platform and reactions were subjected to the following steps: activation for 1 min at 94 °C, denaturation for 15 s at 94 °C, annealing for 30 s at 60-55 °C (decreasing by 1 °C per cycle until 55 °C was reached), extension for 30 s/kbp at 72 °C, repeated for 30 cycles, stored at 4 °C.

2.2.4. Restriction digestion of DNA

Restriction digestions of plasmid DNA and PCR amplified DNA fragments were performed following the instructions of the restriction enzyme manufacturer (New England Biolabs, Ipswich, Massachusetts, USA). For cloning purposes, a typical restriction reaction mixture (50 μ L) contained 10 μ g of plasmid DNA or PCR-amplified DNA, 10-20 units of restriction enzyme and the appropriate amount of digestion buffer and filter-sterilized Milli-Q[®] water. For restriction analysis of clones, a reaction digestion of 10 μ L final volume was set up and the amounts of reagents were adjusted accordingly. The reaction components were mixed thoroughly and incubated at the optimal temperature for 2-3 h. The restricted fragments were separated by agarose gel electrophoresis and visualized under blue light. The molecular size and amount of digested DNA were determined by comparison to marker DNA bands.

2.2.5. Purification of DNA fragments

DNA fragments from restriction enzyme digestions and PCR reactions were purified by a PCR purification protocol or gel extraction method using a QIAquick PCR Purification Kit or a QIAquick Gel Extraction Kit (Qiagen Ltd, Crawley, West Sussex, UK), respectively. The purified DNA was quantified on an agarose gel.

2.2.6. Dephosphorylation of DNA fragments

Dephosphorylation of linearised plasmid DNA was performed according to the manufacturer of calf intestinal alkaline phosphatase (CIAP; Invitrogen, Waltham, Massachusetts, USA). A typical dephosphorylation reaction (50 μ L) was set up by mixing the amount of DNA corresponding to 10 pmol of 5' ends (in 40 μ L), 5 μ L of 10x reaction buffer and 5 μ L of diluted CIAP (1 U/ μ L). Then the dephosphorylation reaction was incubated for 1 h at 50 °C, followed by inactivation of CIAP for 15 min at 65 °C. Dephosphorylated DNA was purified using a QIAquick PCR Purification Kit (Qiagen Ltd, Crawley, West Sussex, UK), and quantified on an agarose gel.

2.2.7. Ligation of DNA fragments

A typical ligation reaction contained 50 ng of restricted vector DNA. Molar vector:insert ratios of 1:1 and 1:3 were used. Ligation was performed in a 10 μ L reaction volume using a LigaFast™ Rapid DNA Ligation System (Promega, Madison, Wisconsin, USA) for 15-30 min at 25 °C. The ligated DNA was transformed into Top10 (Invitrogen, Waltham, Massachusetts, USA) or XL1-Blue (Stratagene, Santa Clara, California, USA) *E. coli* strains.

2.2.8. Preparation of competent *E. coli* cells

Competent *E. coli* cells were prepared by the rubidium chloride method (Promega protocols application guide). Cells were streaked on a LB/agar plate and grown overnight at 37 °C. A single colony was picked and inoculated into 2 mL LB liquid medium and grown overnight at 37 °C with shaking at 200 rpm. From the overnight saturated culture, a 0.5 mL aliquot was transferred to LB liquid medium (50 mL) in a 250 mL shake flask and grown at 37 °C with shaking at 200 rpm until the A_{600} reached 0.4, typically taking 2-3 h. The shake flask containing the cultures was chilled on ice for 5 min and then the cultures were transferred to a pre-chilled 50 mL Falcon tube. The cells were harvested (1000 x g, 4 °C, 10 min) and resuspended in 20 mL of filter-sterilised ice-cold Tfb-I buffer (30 mM potassium acetate, 100 mM rubidium chloride, 10 mM calcium chloride, 50 mM manganese chloride, 15% glycerol; pH adjusted to 5.8 with 0.2 M acetic acid) and placed on ice for 5 min. The cells were then collected by centrifugation (1000 x g, 4 °C, 10 min). The supernatant was discarded, and the cell pellet was resuspended in 2 mL of filter-sterilized Tfb-II buffer (10 mM MOPS, 10 mM rubidium chloride, 75 mM calcium chloride and 15% glycerol; pH adjusted to 6.5 with KOH). The cells were incubated on ice for 15 min, dispensed into 200 μ L aliquots, frozen on dry ice, and then stored at -70 °C.

2.2.9. Transformation of competent *E. coli* cells

A 200 μ L aliquot of competent cells was thawed on ice and equally divided into two 1.5 mL microcentrifuge tubes. Approximately 30 ng plasmid DNA or ligation mixture containing ~30 ng DNA was added to 100 μ L of competent cells and mixed gently. The cells were incubated on ice for 30 min and then heat shocked at 42 °C for 45 s and subsequently incubated on ice for 2 min. To the transformation mixture, 500 μ L of LB medium was added and incubated for 1 h at 37 °C with shaking at 200 rpm. A 200 μ L

aliquot of the transformation mixture was plated on a pre-warmed LB/agar selective plate containing carbenicillin (100 µg/mL) and incubated overnight at 37 °C. Colonies were selected and analysed by colony PCR or plasmid isolation followed by restriction analysis and sequencing.

2.2.10. Automated DNA sequencing

DNA sequence analysis was conducted on an ABI 3130xl capillary sequencer (Applied Biosystems®, Waltham, Massachusetts, USA), using version 3.1 BigDye® terminator cycle sequencing chemistry and a POP7 matrix. DNA was labelled by mixing 200 ng DNA with 3.2 pmol of primers in a 20 µl reaction volume. The reaction mixture was placed in a thermal cycler and subjected to 25 cycles of the following conditions: rapid thermal ramp to 96 °C, denaturation at 96 °C for 10 s, annealing at 50 °C for 5 s, extension at 60 °C for 4 min. The unincorporated dye terminator was removed from the extension products by ethanol/EDTA/sodium acetate extraction.

2.2.11. Amplified expression of recombinant ZitB

The plasmid construct containing the *zitB* gene was transformed into *E. coli* host strain BL21 (Novagen, Lagos, Nigeria). To prepare glycerol stocks (deeps), the *E. coli* liquid culture (800 µL) was mixed with glycerol (80%, 200 µL), then flash frozen in liquid nitrogen and stored at -70 °C. Cells were recovered from frozen deeps by streaking onto LB/agar plates containing carbenicillin (100 µg/mL), which were incubated at 37 °C for 16-18 h. Subsequently, single colonies were transferred to LB liquid medium supplemented with carbenicillin (100 µg/mL) in 50 mL Falcon tubes and incubated overnight at 37 °C with shaking at 200 rpm. Next day cultures were diluted 50-fold (2% inoculum) into 50 mL (for small-scale expression tests) or 500 mL (for large-scale protein production) M9 minimal medium supplemented with 0.2% (w/v) casamino acids, 0.2% (w/v) glycerol and carbenicillin (100 µg/mL) (in 250 mL or 2 litre baffled flasks, respectively) and grown in a shaking incubator at 37 °C and 200 rpm. When the cultures reached an A_{600} of 0.5, expression was induced by the addition of isopropyl-β-D-thiogalactoside (IPTG) (Melford Laboratories Ltd., Ipswich, UK) to a final concentration of 0.25 mM. Growth was continued for a further 3 h, then cells were harvested by centrifugation (12,000 × g, 4 °C, 10 min).

2.2.12. Small-scale preparation of mixed membranes

Small-scale preparations of mixed (inner and outer) membranes used the water lysis method (Witholt et al., 1976; Ward et al., 2000). The cells from 50-mL culture volumes were harvested by centrifugation (12,000 × g, 4 °C, 10 min) and resuspended in 10 mL of 0.2 M Tris-HCl (pH 8.0) in a 50 mL Beckman ultracentrifuge tube (Ti45 rotor). Resuspensions were mixed on a rolling table at room temperature for 20 min. At zero-time, 4.85 mL of sucrose buffer (0.2 M Tris-HCl pH 8.0 containing 1 M sucrose and 1 mM EDTA) was added. At 1.5 min, 65 µl of lysozyme solution (10 mg/mL, freshly prepared in the sucrose buffer) was added and vortexed briefly. At 2 min 9.6 mL of deionised water was added, vortexed briefly and roller mixing continued for 20 min

to allow spheroplast formation. The spheroplasts were collected by ultracentrifugation (Beckman Coulter Optima L-90K) using a pre-cooled Ti45 rotor (45,000 × g, 4 °C, 20 min) and the supernatant (periplasmic fraction) was removed. The spheroplasts were resuspended in 15 mL of deionized water using a homogenizer or a large syringe needle (~ 1 mm × 150 mm) and then shaken for 30 min. The membranes were collected by ultracentrifugation (45,000 × g, 4 °C, 20 min) and the supernatant was discarded. The membranes were washed at least twice by resuspending in 15 mL of 0.1 M sodium phosphate buffer (pH 7.2) containing 1 mM β-mercaptoethanol (β-ME) (as described above) and collected by ultracentrifugation (45,000 × g, 4 °C, 20 min). The membrane pellet was resuspended in 0.2 to 0.4 mL of 0.1 M sodium phosphate buffer (pH 7.2) and mixed with a small syringe needle (~ 0.45 mm × 13 mm) until the suspension became homogenous.

2.2.13. Large-scale preparation of mixed membranes using a cell disruptor

Frozen cells, obtained from large-scale culture volumes (total 5-25 litres), were thawed and resuspended in 20 mM Tris, 1 mM EDTA (pH 7.5) containing 10% glycerol, 1 mM phenylmethylsulfonyl fluoride (PMSF) and cOmplete Protease Inhibitor (one tablet per 8 g wet biomass; Roche Diagnostics, Rotkreuz, Switzerland). Usually, 3-4 mL of buffer per 1 g (wet weight) of cells was used. The suspension was stirred until it was completely homogeneous. Cells were lysed by three passages at 4 °C through a cell disruptor (Constant Systems Ltd., Daventry, Northamptonshire, UK) at 20-30 kpsi. Undisrupted cells and debris were sedimented by centrifugation (12,000 × g, 4 °C, 30 min). The supernatant was transferred to 50 mL ultracentrifuge tubes (Ti45 rotor) and membranes were collected by ultracentrifugation (131,000 × g, 4 °C, for 2 h). Membranes were washed twice with 20 mM Tris-HCl (pH 7.5) buffer to remove the EDTA by the same procedure as described above. Membranes were resuspended in an appropriate volume of 20 mM Tris (pH 7.5) buffer to give a final protein concentration in the range of 20-30 mg/mL, then dispensed into aliquots (0.3-0.5 mL), flash frozen in liquid nitrogen, and stored at -70 °C.

2.2.14. Separation of inner and outer membrane fractions by sucrose density gradient ultracentrifugation

Mixed membranes, as prepared above, were resuspended in 5 mL of Tris-EDTA buffer (20 mM Tris-HCl, 0.5 mM EDTA, pH 7.5) containing 25% sucrose and then carefully transferred to the top of a step gradient of sucrose (10 mL each of 55%, 50%, 45%, 40%, 35% and 30% sucrose in Tris-EDTA buffer pH 7.5) in a Ti45 ultracentrifuge tube (Beckman) held on ice. Inner and outer membranes were separated by ultracentrifugation (113,000 × g, 4 °C, 18 h) with minimal acceleration and no braking. When centrifugation was completed, the inner (golden band in the 30-40% zone) and the outer (white band in the 45-55% zone) membrane fractions were carefully recovered using clean syringes and transferred to separate tubes. Membranes were washed three-times with Tris-EDTA buffer to remove the sucrose, collecting by ultracentrifugation (113,000 × g, 4 °C, 18 h) after each wash. The resultant membrane

pellet was resuspended in an appropriate volume and dispensed into 0.3 mL aliquots, which were flash frozen in an ethanol bath at -70 °C and stored at -70 °C.

2.2.15. Purification of ZitB

Inner membranes containing 30 mg total protein were solubilised by incubation on ice for 1.5 h in 6 mL 20 mM Tris-Cl (pH 7.9) containing 100 mM NaCl, 20% (v/v) glycerol, 4 mM β -ME, 5 mM imidazole and 1% (w/v) *n*-dodecyl- β -D-maltopyranoside (DDM) (Melford Laboratories Ltd., Ipswich, UK). Insoluble material was removed by ultracentrifugation (100,000 x g, 4 °C, 1 h), then the supernatant was gently mixed for 3 h at 4 °C with 1 mL Ni-NTA agarose (50% suspension) (Qiagen, UK), which was pre-equilibrated with wash buffer [20 mM Tris-Cl (pH 7.9) containing 300 mM NaCl, 10% (v/v) glycerol, 2 mM β -ME, 30 mM imidazole and 0.05% (w/v) DDM]. After packing into a column, the agarose was washed with 40-column volumes of wash buffer. ZitB was eluted from the column in 20 mM Tris-Cl (pH 7.9) containing 100 mM NaCl, 10% (v/v) glycerol, 2 mM β -ME, 500 mM imidazole and 0.05% (w/v) DDM. The purified protein was placed into a 10 kDa cutoff dialysis cassette (Pierce Biotechnology, Rockford, Illinois, USA) and dialysed overnight against 20 mM Tris-HCl (pH 7.9), containing 100 mM NaCl, 10% (v/v) glycerol, 2 mM β -ME and 0.05% (w/v) DDM, then concentrated to 10-15 mg/mL using a 50 kDa cut-off Vivaspin® concentrator (Sartorius, Göttingen, Germany) (centrifugation at 3,000 x g and 4 °C).

2.2.16. Determination of protein concentration

Protein concentration was determined by the bicinchoninic acid (BCA) assay (Pierce Biotechnology, Rockford, Illinois, USA) using a microplate procedure according to the manufacturer's instructions using bovine serum albumin (BSA) (Merck, Darmstadt, Germany) as the standard. Protein samples were diluted where necessary to fall within the standard protein concentrations range (2-10 μ g). Standard and sample solutions were added into microplate wells in duplicate followed by the addition of 200 μ L assay reagent. The assay reagent was prepared by mixing 50:1 of BCA reagent (Pierce Biotechnology, Rockford, Illinois, USA) and 4% CuSO₄. The plate was incubated at 37 °C for 30 min to allow colour development (purple). The absorbance was measured at 570 nm using a Titertek Fluoroskan II Microplate Reader (ICN Biomedicals, Irvine, California, USA). The protein concentration of unknown samples was measured from the linear graph which was obtained by plotting the known standard concentrations against relevant absorbance.

2.2.17. Protein analysis by SDS-PAGE

Sodium dodecylsulphate polyacrylamide gel electrophoresis (SDS-PAGE) (Laemmli, 1970) was performed on a Mini PROTEAN II apparatus (Bio-Rad, Hercules, California, USA) using a 10% separating gel and a 3% stacking gel. Membrane samples containing 5, 10 or 20 μ g total protein were diluted to 15 μ L with distilled water. Sample loading buffer [5.4 M glycerol, 10% SDS, 10 mM EDTA, in Tris-HCl (0.5 M, pH

6.8) + Pyronin Y] (5 μ L) and 100 mM dithiothreitol (1 μ L) were added with brief vortexing, then the solutions were held at room temperature for 30 min before loading into lanes of the gel. Electrophoresis was performed at constant voltage (100 V) using running buffer (190 mM glycine, 25 mM Tris-HCl, 0.1% SDS, in Milli-Q[®] water) until the dye front reached the bottom of the gel (~90 min). Protein bands were visualised by Coomassie Blue staining, as follows. The gel was soaked sequentially on an orbital platform in fixing solution (65:25:10 water/2-propanol/glacial acetic acid) for ~3 h, staining solution (65:25:10 water/2-propanol/glacial acetic acid containing 0.025% Coomassie Brilliant Blue R-250) for ~20 h, and then several changes of destaining solution (90:10 water/glacial acetic acid) over ~24 h or until the background was faded sufficiently.

2.2.18. Mass spectrometry

Using ~300 μ g of purified ZitB, salts were removed by dialysis against 3-4 litres of Milli-Q[®] water for 2-3 days using 10-30 kDa molecular weight cut-off dialysis tubing, and the water was changed every day. Sometimes the protein precipitated during the dialysis procedure, in this case it was collected by centrifugation (13,000 \times g, 4 $^{\circ}$ C, 10-15 min), then stored at -20 $^{\circ}$ C until analysis. When the protein remained in solution following dialysis, it was concentrated to 2-3 mg/mL using a 30 kDa cut-off Vivaspin[®] concentrator (Sartorius, Göttingen, Germany) (centrifugation at 3,000 \times g and 4 $^{\circ}$ C). The molecular mass of purified ZitB was determined using a surface enhanced laser desorption ionization mass spectrometer (SELDI MS; Ciphergen Biosystems, Fremont, California, USA). The protein concentration used was typically in the range 20-30 μ M. The precipitated protein from dialysis was dissolved in 10-15 μ L of 60% formic acid. The dissolved protein in 60% formic acid, or protein that had remained water-soluble following dialysis, was diluted 1:1 in sinipinic matrix (Ciphergen Biosystems, Fremont, California, USA), prepared in a 2:1:1 mixture of acetonitrile/water/TFA (2%). A 2 μ L aliquot of protein-matrix solution was placed on a chip and analysed by SELDI-MS. Analysis was performed within 5-10 min of protein dissolution/dilution in 60% formic acid to prevent adventitious formylation. The instrument was calibrated using protein standards of known molecular mass: bovine serum albumin (66433), rabbit GAPDH (35688); equine cardiac myoglobin (16951), equine cardiac cytochrome C (12360.2).

2.2.19. Circular dichroism (CD) spectroscopy

Far-UV CD measurements were performed using a CHIRASCAN instrument (Applied Photophysics Ltd., Leatherhead, UK) at 20 $^{\circ}$ C with constant nitrogen flushing. Purified ZitB was concentrated to 0.5-1 mg/mL using a 30 kDa cut-off Vivaspin[®] concentrator (Sartorius, Göttingen, Germany) (centrifugation at 3,000 \times g and 4 $^{\circ}$ C) and then exchanged into 10 mM potassium phosphate buffer (pH 7.4), containing 0.05% DDM using the same concentrator. Samples (300 μ L) containing the purified protein at a concentration of 0.02 mg/mL were added into a quartz cuvette of 1 mm pathlength (Hellma, Müllheim, Germany). Data were recorded over the

wavelength range 190 to 260 nm at a scan speed of 1 nm/s. Spectra were obtained by averaging the data from ten accumulations. A blank sample containing only the buffer was scanned in the same way, and the blank spectrum was subtracted from the protein sample spectrum. Arbitrary CD ellipticity values were converted to mean residue ellipticity (MRE) ($\text{deg.cm}^{-2}.\text{dmol}^{-1}$).

3. Analytical Review, Results and Discussion

3.1. Functional and structural properties of ZitB

ZitB was first identified as a zinc exporter in 2001, when it was observed that a *zitB*-deleted strain of *E. coli* (GG48; $\Delta\text{zitB}::\text{Cm zntA}::\text{Km}$) was more zinc sensitive than the parent strain (RW3110; *zntA*::Km) (Grass et al., 2001). Induction of *zitB* on a pASK-IBA3-derived plasmid in *E. coli* strain GG48 by addition of anhydrotetracycline produced a significant increase in zinc resistance, whilst there was no significant resistance to cobalt or cadmium. (Grass et al., 2001). When the *zitB* gene was carried on a different plasmid that was transformed into *E. coli*, *zitB* expression was strongly induced by zinc and slightly induced by cadmium, whilst other metals (cobalt, nickel, copper) did not produce significant induction. Induction of *zitB* was observed with 50 μM ZnCl_2 and reached a maximum at 100 μM , whilst higher concentrations produced a decrease of *zitB* expression. It was postulated that ZitB contributes to zinc homeostasis at low concentrations of zinc, while ZntA is required for growth at higher and more toxic concentrations (Grass et al., 2001). Indeed, based on a experiments using a genetically-encoded fluorescent zinc sensor to monitor the intracellular free zinc changes in wild type, ΔzitB and ΔzntA *E. coli* cells upon sudden exposure to toxic levels of zinc, it was concluded that ZitB serves as a constitutive, first-line defence against toxic zinc influx, while ZntA is up-regulated to efficiently lower the free zinc concentration (Wang et al., 2012).

The first kinetic study of purified and reconstituted ZitB was conducted by stopped-flow measurements of transmembrane fluxes of metal ions (Zn^{2+} and Cd^{2+}) using the metal-sensitive fluorescent indicator fluozin-1 encapsulated in proteoliposomes (Chao and Fu, 2004). In metal ion filling experiments, the initial rate of Zn^{2+} influx was a linear function of the molar ratio of ZitB to lipid. Influx corresponded to the concentration of Zn^{2+} (0-4 mM) or Cd^{2+} (0-2 mM) ions in a hyperbolic manner with Michaelis-Menten constants (K_m) of 104.9 +/- 5.4 μM and 90.1 +/- 3.7 μM , respectively (Chao and Fu, 2004). Thus, both Zn^{2+} and Cd^{2+} were demonstrated to be effective substrates of ZitB. When a proposed antiport mechanism for ZitB was tested using a proteoliposome system, tetraethylammonium ion substitution for K^+ did not affect Cd^{2+} transport, so it was demonstrated that Cd^{2+} transport by ZitB was not coupled to K^+ ions (Chao and Fu, 2004). In contrast, depletion of H^+ stalled Cd^{2+} transport down its diffusion gradient, suggesting that H^+ is the coupling ion for ZitB. This was confirmed by observing a H^+ concentration dependence of Cd^{2+} transport that had a hyperbolic relationship with a K_m of 19.9 nm for H^+ . Applying H^+ diffusion gradients across the membrane caused Cd^{2+} fluxes both

into and out of proteoliposomes against the H^+ gradients. Similarly, the application of an outwardly oriented membrane electrical potential resulted in Cd^{2+} efflux. Overall, the results demonstrated an electrogenic effect of ZitB transport, where ZitB is an antiporter catalyzing the exchange of Zn^{2+} or Cd^{2+} for H^+ with a likely exchange stoichiometry of 1:1 (Chao and Fu, 2004). In a different study, ZitB transported $^{65}Zn^{2+}$ into everted membrane vesicles only in the presence of NADH, thus confirming that ZitB is driven by the PMF. The ZitB-dependent $^{65}Zn^{2+}$ transport had an apparent K_m of $1.4 \mu M$ and a V_{max} of $0.57 \text{ nmol of } Zn^{2+} \text{ min}^{-1} \text{ mg of protein}^{-1}$ (Anton et al., 2004). Solid-state NMR measurements in native membranes and fluorescence-based (fluozin-1) transport measurements in proteoliposomes confirmed that ZitB can bind and export Zn^{2+} and Cd^{2+} ions, and possibly also Zn^{2+} and Cd^{2+} (Rahman et al., 2008).

ZitB from *E. coli* strain K12 (UniProt: P75757) is comprised from 313 amino acids and has a predicted molecular weight of 34,678 Da. Analysis of the ZitB sequence by the online topology prediction tools DeepTMHMM (<https://dtu.biolib.com/DeepTMHMM>) (Hallgren et al., 2022) and TOPCONS (<https://topcons.cbr.su.se/>) (Tsirigos et al., 2015) both predict that ZitB contains six transmembrane α -helices (21-41, 51-68, 88-110, 125-142, 160-179, 187-202 and 22-42, 53-73, 87-107, 122-142, 159-179, 185-205, respectively) with both the N- and C-terminal ends at the cytoplasmic side of the membrane, as expected for CDF family proteins. Looking at the amino acid composition of ZitB, it is noticeable that it has a significantly high histidine content (8.0%) compared to YiiP (3.0%) and to the average content in 235 secondary transport proteins from *E. coli* (1.4%) (Saidijam and Patching, 2015) (Figure 3). The human ZnTs (1-10) have histidine contents of 4.1%, 4.6%, 4.4%, 3.0%, 5.1%, 2.4%, 7.2%, 3.5%, 1.8% and 2.3%, respectively.

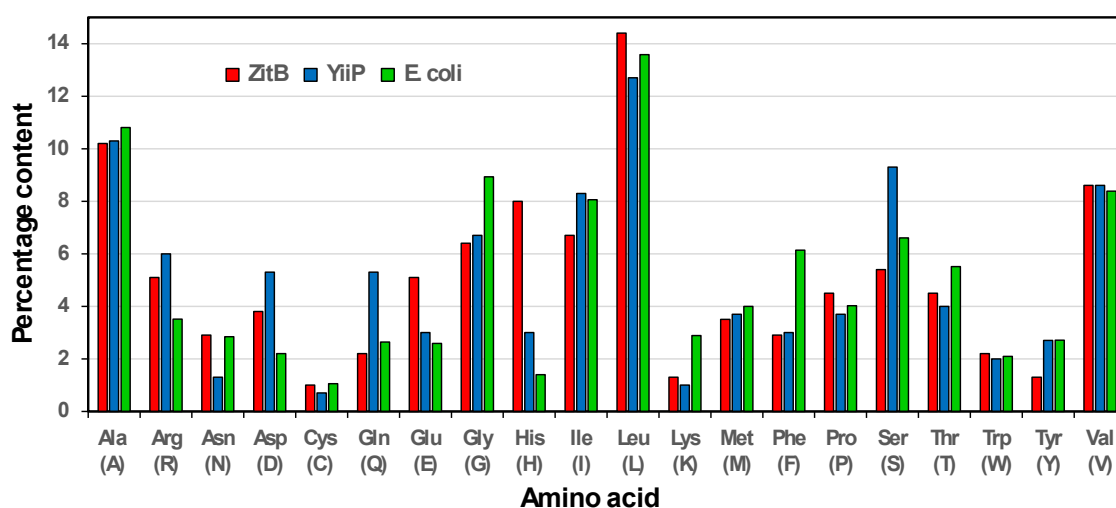


Figure 3. Amino acid compositions of ZitB and YiiP. The amino acid sequences of ZitB (P75757) and YiiP (P69380) were taken from the UniProt Knowledgebase (<https://www.uniprot.org/>) and the percentage content of individual amino acid types in each protein were calculated using the ExPASy tool ProtParam (<https://web.expasy.org/protparam/>) (Gasteiger et al., 2005). Values for ZitB (red) and YiiP (blue) were compared with the average contents in 235 *E. coli* secondary transport proteins (Saidijam and Patching, 2015) (green).

When the amino acid sequences of ZitB and YiiP were aligned, they shared 21% identically conserved residues (Figure 4). Interestingly, ZitB shared a greater number of identically conserved residues with human ZnTs (1-10) of 38.87%, 33.99%, 34.31%, 33.99%, 29.97%, 24.60%, 27.40%, 34.10%, 21.50% and 33.11%, respectively, which was also seen in the phylogenetic analysis (Figure 1). In the sequence alignment between ZitB and YiiP we have also highlighted YiiP residues that constitute transmembrane α -helices, C-terminal α -helices and C-terminal β -strands based on its crystal structure, YiiP residues involved in zinc binding sites, histidine residues in ZitB and residues in ZitB that have been subjected to site-directed mutation studies (Figure 4).

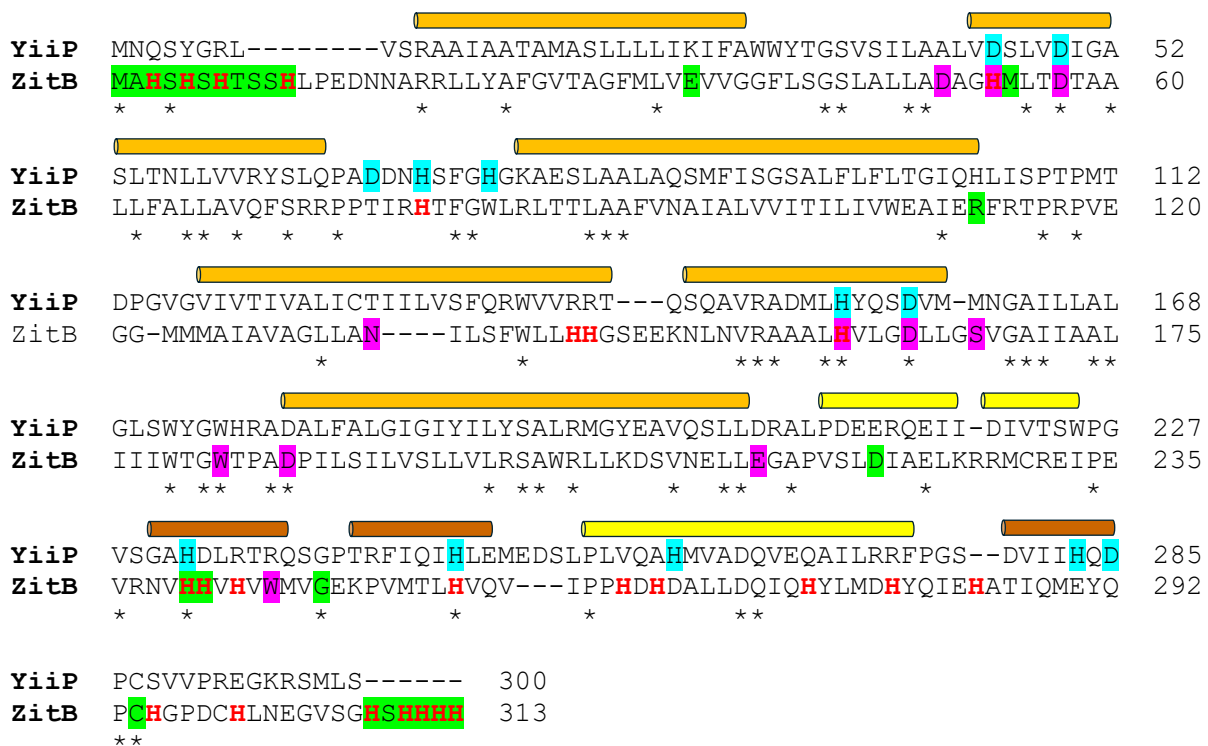


Figure 4. Sequence and structural features of ZitB compared with YiiP. The amino acid sequences of ZitB (P75757) and YiiP (P69380) were taken from the UniProt Knowledgebase (<https://www.uniprot.org/>) and aligned using the online tool MUSCLE (<https://www.ebi.ac.uk/jdispatcher/msa/muscle?style=protein>) (Madeira et al., 2024). Residues identically conserved between ZitB and YiiP (63 residues = 21%) are indicated by asterisks (*). Residues in YiiP that constitute transmembrane α -helices (TMH I-VI) (orange bars), C-terminal α -helices (CTH 1-3) (yellow bars) and C-terminal β -strands (CTS 1-3) (brown bars), based on the crystal structure of YiiP (PDB 3H90), are indicated above the sequence for YiiP. Residues involved in zinc binding sites in YiiP are also indicated (cyan). In the sequence for ZitB, the following residues are indicated: histidine residues (red), individual mutation of this residue abolishes activity or results in partial activity (pink), individual mutation of this residue or removal of this sequence does not affect activity or has a slight effect on activity (green). Mutation results are based on studies by Lee et al. (2002) and Anton et al. (2004).

Two different studies performed some site-directed mutational analysis of ZitB, where the effects of mutations were monitored by measuring zinc resistance and zinc uptake (Lee et al., 2002; Anton et al., 2004). Mutations at H53 and D57 in TMHII, and H159 and D163 in TMHV (H53R, D57A, H159R, H159E, D163A, D163E) resulted in abolished ZitB function. These positions correspond to the four residues (D45, D49, H153 and D157, respectively) in zinc binding site A of YiiP (Figure 4). In a highly conserved region of TMHII (DAXHMLTD, residues 50-57), mutant D50E was partially active and D50A had no function. In TMHVI, mutant D186A had abolished function, which corresponds to the conserved D179 in YiiP. ZitB mutant E214A did not confer zinc resistance, this position corresponds to D207 in YiiP. Mutations N135A and S167A also resulted in abolished ZitB function, which correspond to YiiP residues T128 and M160, respectively (Figure 4). Mutations at two tryptophan residues (W182L and W245L) resulted in partial activity, so they are not essential for ZitB function. Single-site mutations of further residues had no effect (R112, D221, H240, H241, C294) or a slight effect (E35, M54, G248) on ZitB function, so these can also be considered as non-essential (Lee et al., 2002; Anton et al., 2004). The study by Lee et al. (2002) demonstrated that the histidine-rich amino terminal (MAHSHSHTSSH, residues 1-11) and carboxy-terminal (HSHHHH, residues 308-313) regions of ZitB were not required for function (Figure 4). Indeed, ZitB function was not affected by removal of the C-terminal residues 294-313, which includes the cysteines C294 and C299. A double deletion at both the N-terminus (residues 1-11) and C-terminus (residues 294-313) did result in loss of ZitB function, but it also did not produce a cross-reacting protein in expression tests (Lee et al., 2002).

3.2. Amplified expression and purification of ZitB

To provide sufficient quantities of protein for further structural and functional characterisation of ZitB, we employed the expression plasmid pTTQ18 (Stark, 1987), which has successfully been used to amplify the expression of various bacterial membrane proteins in *E. coli* (Saidijam et al., 2003; Saidijam et al., 2005; Clough et al., 2006; Ma et al., 2008; Henderson et al., 2009; Bettaney et al., 2013; Ma et al., 2016; Rahman et al., 2017; Ahmad et al., 2020; Ahmad et al., 2021; Ahmad et al., 2022). In this IPTG-inducible plasmid, expression of the inserted gene of interest is under control of the strong hybrid *trp-lac* (*tac*) promoter and the *rrnB* transcription terminator. A non-tagged, wild-type form of the *E. coli zitB* gene was inserted into the multicloning site of pTTQ18 by introducing *EcoR1* and *Pst1* restriction sites at its 5' and 3' ends, respectively (Figure 5A). Successful recombinant clones in *E. coli* strain BL21 were identified by colony PCR, giving amplified DNA fragments with a size of ~1.2 Kb (expected 1155 bases, *zitB* gene plus 216 vector-derived nucleotides) (Figure 5B). In membrane preparations from these cells, IPTG-induced amplified expression of the monomeric form of ZitB was clearly observed by SDS-PAGE analysis, giving a band with a molecular weight position of ~30 kDa (Figure 5C). The ZitB content in inner membrane preparations was ~15% of total protein according to densitometric analysis of the Coomassie-stained gel.

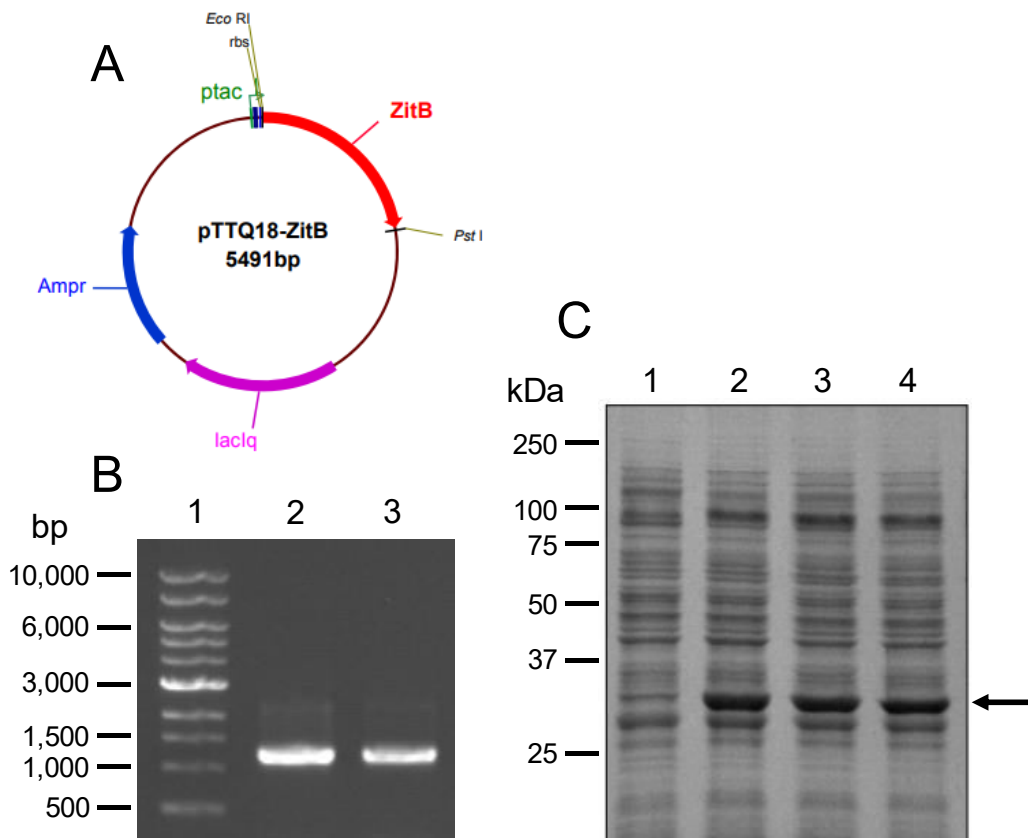


Figure 5. Cloning and amplified expression of non-tagged wild-type ZitB. **A.** Map of vector pTTQ18-ZitB for amplifying expression of the *zitB* gene under control of the tac promoter (ptac). lacIq = gene encoding the lac repressor, Ampr = gene encoding β -lactamase responsible for ampicillin resistance, rbs = ribosomal binding site. **B.** Agarose gel identifying colonies harbouring pTTQ18-ZitB by colony PCR. Lane 1 contains a 1 Kb DNA ladder with sizes indicated. Lanes 2 and 3 show the ~1.2 Kb PCR-amplified DNA fragments (encoding *zitB* plus vector-derived sequences) from two representative positive recombinant colonies. **C.** Amplified expression of ZitB in *E. coli* BL21 cells harbouring plasmid pTTQ18-ZitB. Samples of mixed membrane preparations containing 20 μ g protein from uninduced cells (lane 1) and from cells induced with 0.25, 0.5 and 1.0 mM IPTG (lanes 2-4, respectively) were subjected to SDS-PAGE followed by Coomassie blue staining. The positions of molecular weight standards are shown on the left and the position of the amplified monomeric form of ZitB is indicated by an arrow.

Purification of this non-tagged form of ZitB was achieved by immobilised metal affinity chromatography (IMAC) by exploiting the high histidine content in the native protein, including the five histidines at the C-terminus. From large scale cultures of *E. coli* expressing ZitB, inner membranes were isolated and then solubilised in the mild detergent *n*-dodecyl- β -*D*-maltoside (DDM). The purification was monitored by SDS-PAGE (Figure 6A) and it typically produced purified ZitB in yields of ~1.8 mg/litre. Mass spectrometry analysis of the purified ZitB produced a molecular ion with a mass of 34686.7 (expected 34678) (Figure 6B), and far-UV circular dichroism analysis produced a spectrum consistent with α -helical secondary structure (Figure 6C).

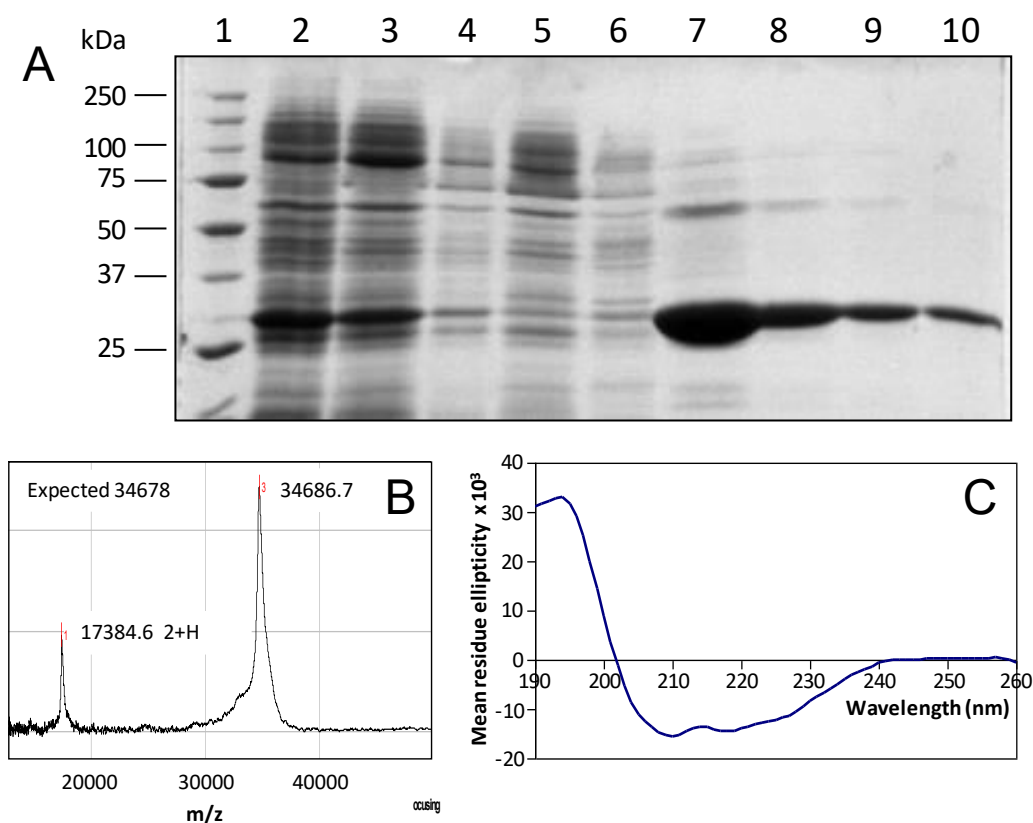


Figure 6. Purification of non-tagged wild-type ZitB. **A.** SDS-PAGE analysis of ZitB amplified expression and purification by Ni-NTA affinity chromatography. The lanes on the gel were loaded with the following samples: 1. Molecular weight markers, 2. *E. coli* inner membranes with amplified expression of non-tagged wild-type ZitB, 3. Soluble fraction from membranes following solubilisation with DDM (supernatant), 4. Insoluble fraction from membranes (pellet), 5. Unbound fraction from Ni-NTA column, 6. Wash from Ni-NTA column (30 mM imidazole), 7-10. Eluted fractions from column (500 mM imidazole). **B.** Mass spectrometry (SELDI-MS) analysis of purified ZitB. **C.** Far-UV circular dichroism analysis of purified ZitB.

4. Conclusion and Future Directions

The *E. coli* zinc exporter ZitB is one of the best characterised CDF proteins using various biochemical and computational methods, which we have reviewed and expanded on in this work. A high-resolution three-dimensional structure of ZitB has not yet been elucidated, however. We have so far resisted constructing a homology model of ZitB based on the existing structures of other CDF proteins, instead preferring to strive for a high-resolution structure of ZitB. In the journey to achieve this, the gene for *E. coli* ZitB was successfully cloned into plasmid pTTQ18 and amplified expression of a non-tagged form of ZitB in *E. coli* was achieved at a level of ~15% of total protein in inner membrane preparations. ZitB was successfully solubilised using the mild detergent DDM and purified in yields of ~1.8 mg/litre. Purified ZitB had structural integrity according to mass spectrometry and circular dichroism analyses, thus making it a promising candidate for high-resolution structure determination. To further demonstrate the suitability of ZitB for structure and function studies using different chemical, biochemical and biophysical

techniques, the thermal stability of purified ZitB reconstituted in different detergents and lipids should be rigorously tested. Further mutagenesis studies of ZitB should help to better understand the roles of specific residues in the molecular mechanism of ZitB in comparison to other CDF proteins.

Conflict of Interest

The authors have no conflicts of interest to declare.

References

- Acevedo S, Segovia MF, de la Fuente-Ortega E. Emerging perspectives in zinc transporter research in prostate cancer: An updated review. *Nutrients* 2024; 16(13): 2026.
- Ahmad I, Hassan KA, Henderson PJF, Patching SG. Cloning, amplified expression, functional characterisation and purification of a *Pseudomonas putida* NCS1 family transport protein. *Int J Adv Multidiscip Res* 2022; 9(12): 127-156.
- Ahmad I, Lee Y, Nawaz N, Elahi R, Khan IA, Mustafa MZ, Patching SG. Cloning, amplified expression and bioinformatics analysis of a putative Nucleobase Cation Symporter-1 (NCS-1) protein from *Rhodococcus erythropolis*. *BioScientific Review* 2021; 3(4). DOI: 10.32350//BSR.0304.05
- Ahmad I, Ma P, Nawaz N, Sharples DJ, Henderson PJF, Patching SG. Cloning, amplified expression, functional characterisation and purification of *Vibrio parahaemolyticus* NCS1 cytosine transporter VPA1242. Chapter 8. In: Patching SG (Ed), *A Closer Look at Membrane Proteins*, 2020. Independent Publishing Network, UK, pp. 241-267. ISBN: 978-1-83853-535-3.
- Ahmad I, Nawaz N, Darwesh NM, Ur Rahman S, Mustafa MZ, Khan SB, Patching SG. Overcoming challenges for amplified expression of recombinant proteins using *Escherichia coli*. *Protein Expr Purif* 2018; 144: 12-18.
- Alav I, Kobylka J, Kuth MS, Pos KM, Picard M, Blair JMA, Bavro VN. Structure, assembly, and function of tripartite efflux and type 1 secretion systems in Gram-negative bacteria. *Chem Rev* 2021; 121(9): 5479-5596.
- Alluri K, Nair KPM, Ghosh S. Differential expression of zinc transporters in functionally contrasting tissues involved in zinc homeostasis. *Nucleosides Nucleotides Nucleic Acids* 2020; 39(4): 615-629.
- Andreini C, Banci L, Bertini I, Rosato A. Zinc through the three domains of life. *J Proteome Res* 2006; 5(11): 3173-3178.
- Anton A, Weltrowski A, Haney CJ, Franke S, Grass G, Rensing C, Nies DH. Characteristics of zinc transport by two bacterial cation diffusion facilitators from *Ralstonia metallidurans* CH34 and *Escherichia coli*. *J Bacteriol* 2004; 186(22): 7499-7507.
- Baltaci AK, Mogulkoc R, Baltaci SB. Review: The role of zinc in the endocrine system. *Pak J Pharm Sci* 2019; 32(1): 231-239.
- Baltaci AK, Yuce K. Zinc transporter proteins. *Neurochem Res* 2018; 43(3): 517-530.

- Barber-Zucker S, Moran A, Zarivach R. Metal transport mechanism of the cation diffusion facilitator (CDF) protein family - A structural perspective on human CDF (ZnT)-related diseases. *RSC Chem Biol* 2021; 2(2): 486-498.
- Bettaney KE, Sukumar P, Hussain R, Siligardi G, Henderson PJ, Patching SG. A systematic approach to the amplified expression, functional characterization and purification of inositol transporters from *Bacillus subtilis*. *Mol Membr Biol* 2013; 30(1): 3-14.
- Bin BH, Seo J, Kim ST. Function, structure, and transport aspects of ZIP and ZnT zinc transporters in immune cells. *J Immunol Res* 2018; 2018: 9365747.
- Brion LP, Heyne R, Lair CS. Role of zinc in neonatal growth and brain growth: Review and scoping review. *Pediatr Res* 2021; 89(7): 1627-1640.
- Bui HB, Watanabe S, Nomura N, Liu K, Uemura T, Inoue M, Tsutsumi A, Fujita H, Kinoshita K, Kato Y, Iwata S, Kikkawa M, Inaba K. Cryo-EM structures of human zinc transporter ZnT7 reveal the mechanism of Zn²⁺ uptake into the Golgi apparatus. *Nat Commun* 2023; 14: 4770.
- Campoy S, Jara M, Busquets N, Pérez De Rozas AM, Badiola I, Barbé J. Role of the high-affinity zinc uptake znuABC system in *Salmonella enterica* serovar typhimurium virulence. *Infect Immun* 2002; 70(8): 4721-4725.
- Chao Y, Fu D. Thermodynamic studies of the mechanism of metal binding to the *Escherichia coli* zinc transporter YiiP. *J Biol Chem* 2004; 279(17): 17173-17180.
- Choudhury R, Srivastava S. Zinc resistance mechanisms in bacteria. *Current Science* 2001; 81(7): 768-775.
- Clough J, Saidijam M, Bettaney KE, Szakonyi G, Patching SG, Mueller J, Shibayama K, Bacon M, Barksby E, Groves M, Herbert RB, Phillips-Jones M, Ward A, Gunn-Moore F, O'Reilly J, Rutherford NG, Bill R, Henderson PJF. Prokaryotic membrane transport proteins: amplified expression and purification. In: Lundstrom KH (Ed), *Structural genomics on membrane proteins*, 2006. Taylor and Francis, pp. 21-42.
- Consales A, Agostoni C, Cazzola R, Ottria R, Gianni ML. Tracing zinc's role in preterm infants' health: A narrative review. *Adv Nutr* 2024; 15(12): 100295.
- Cotrim CA, Jarrott RJ, Martin JL, Drew D. A structural overview of the zinc transporters in the cation diffusion facilitator family. *Acta Crystallogr D Struct Biol* 2019; 75(Pt 4): 357-367.
- Cuajungco MP, Ramirez MS, Tolmasky ME. Zinc: Multidimensional effects on living organisms. *Biomedicines* 2021; 9(2): 208.
- Cuevas LE, Koyanagi A. Zinc and infection: A review. *Ann Trop Paediatr* 2005; 25(3): 149-160.
- Daniels MJ, Jagielnicki M, Yeager M. Structure/function analysis of human ZnT8 (SLC30A8): A diabetes risk factor and zinc transporter. *Curr Res Struct Biol* 2020; 2: 144-155.
- Davidson HW, Wenzlau JM, O'Brien RM. Zinc transporter 8 (ZnT8) and β cell function. *Trends Endocrinol Metab* 2014; 25(8): 415-424.

- Eide DJ. The SLC39 family of metal ion transporters. *Pflugers Arch* 2004; 447(5): 796-800.
- Fallah A, Mohammad-Hasani A, Colagar AH. Zinc is an essential element for male fertility: A review of Zn roles in men's health, germination, sperm quality, and fertilization. *J Reprod Infertil* 2018; 19(2): 69-81.
- Frassinetti S, Bronzetti G, Caltavuturo L, Cini M, Croce CD. The role of zinc in life: A review. *J Environ Pathol Toxicol Oncol* 2006; 25(3): 597-610.
- Gasteiger E, Hoogland C, Gattiker A, Duvand S, Wilkins MR, Appel RD, Bairoch A. Protein identification and analysis tools on the ExPASy server. In: Walker JM (Ed) *The proteomics protocols handbook*, 2005. Springer Protocols Handbooks. Humana Press. <https://doi.org/10.1385/1-59259-890-0:571>
- Grass G, Fan B, Rosen BP, Franke S, Nies DH, Rensing C. ZitB (YbgR), a member of the cation diffusion facilitator family, is an additional zinc transporter in *Escherichia coli*. *J Bacteriol* 2001; 183(15): 4664-4667.
- Grass G, Franke S, Taudte N, Nies DH, Kucharski LM, Maguire ME, Rensing C. The metal permease ZupT from *Escherichia coli* is a transporter with a broad substrate spectrum. *J Bacteriol* 2005; 187(5): 1604-1611.
- Grass G, Wong MD, Rosen BP, Smith RL, Rensing C. ZupT is a Zn(II) uptake system in *Escherichia coli*. *J Bacteriol* 2002; 184(3): 864-866.
- Hallgren J, Tsigos KD, Pedersen MD, Almagro Armenteros JJ, Marcatili P, Nielsen H, Krogh A, Winther O. DeepTMHMM predicts alpha and beta transmembrane proteins using deep neural networks. *bioRxiv* 2022. DOI: 10.1101/2022.04.08.487609.
- Haney CJ, Grass G, Franke S, Rensing C. New developments in the understanding of the cation diffusion facilitator family. *J Ind Microbiol Biotechnol* 2005; 32(6): 215-226.
- Hara T, Yoshigai E, Ohashi T, Fukada T. Zinc transporters as potential therapeutic targets: An updated review. *J Pharmacol Sci* 2022; 148(2): 221-228.
- Henderson PJF, Suzuki S, Ma P, Saidijam M, Bettaney K, Szakonyi G, Rutherford NG, Patching SG, Hope RJ, Roach PCJ, Shimamura T, Yajima S, Carpenter EP, Weyand S, Cameron A, Iwata S. Structural genomics of bacterial membrane transport proteins. *Acta Crystallographica Section A - Foundations of Crystallography* 2009; 65(a1): s28
- Huang L, Tepasamorndech S. The SLC30 family of zinc transporters - A review of current understanding of their biological and pathophysiological roles. *Mol Aspects Med* 2013; 34(2-3): 548-560.
- Huang T, Yan G, Guan M. Zinc homeostasis in bone: Zinc transporters and bone diseases. *Int J Mol Sci* 2020; 21(4): 1236.
- Hussein A, Fan S, Lopez-Redondo M, Kenney I, Zhang X, Beckstein O, Stokes DL. Energy coupling and stoichiometry of Zn²⁺/H⁺ antiport by the prokaryotic cation diffusion facilitator YiiP. *Elife* 2023; 12: RP87167.

- Ishida H, Yo R, Zhang Z, Shimizu T, Ohto U. Cryo-EM structures of the zinc transporters ZnT3 and ZnT4 provide insights into their transport mechanisms. *FEBS Lett* 2025; 599(1): 41-52.
- Jeong J, Eide DJ. The SLC39 family of zinc transporters. *Mol Aspects Med* 2013; 34(2-3): 612-619.
- Kambe T, Tsuji T, Hashimoto A, Itsumura N. The physiological, biochemical, and molecular roles of zinc transporters in zinc homeostasis and metabolism. *Physiol Rev* 2015; 95(3): 749-784.
- Kavanaugh LG, Dey D, Shafer WM, Conn GL. Structural and functional diversity of Resistance-Nodulation-Division (RND) efflux pump transporters with implications for antimicrobial resistance. *Microbiol Mol Biol Rev* 2024; 88(3): e0008923.
- Kawasaki E. ZnT8 and type 1 diabetes. *Endocr J* 2012; 59(7): 531-537.
- Kiouri DP, Tsoupra E, Peana M, Perlepes SP, Stefanidou ME, Chasapis CT. Multifunctional role of zinc in human health: An update. *EXCLI J* 2023; 22: 809-827.
- Kolaj-Robin O, Russell D, Hayes KA, Pembroke JT, Soulimane T. Cation Diffusion Facilitator family: Structure and function. *FEBS Lett* 2015; 589(12): 1283-1295.
- Krebs NF, Miller LV, Hambidge KM. Zinc deficiency in infants and children: A review of its complex and synergistic interactions. *Paediatr Int Child Health* 2014; 34(4): 279-288.
- Laemmli UK. Cleavage of structural proteins during the assembly of the head of bacteriophage T4. *Nature* 1970; 227(5259): 680-685.
- Lee SM, Grass G, Haney CJ, Fan B, Rosen BP, Anton A, Nies DH, Rensing C. Functional analysis of the *Escherichia coli* zinc transporter ZitB. *FEMS Microbiol Lett* 2002; 215(2): 273-278.
- Letunic I, Bork P. Interactive Tree Of Life (iTOL): An online tool for phylogenetic tree display and annotation. *Bioinformatics* 2007; 23(1): 127-128.
- Lopez-Redondo ML, Coudray N, Zhang Z, Alexopoulos J, Stokes DL. Structural basis for the alternating access mechanism of the cation diffusion facilitator YiiP. *Proc Natl Acad Sci U S A* 2018; 115(12): 3042-3047.
- Lu, M, Chai J, Fu D. Structural basis for autoregulation of the zinc transporter YiiP. *Nat Struct Mol Biol* 2009; 16(10): 1063-1067.
- Lu M, Fu D. Structure of the zinc transporter YiiP, *Science* 2007; 317(5845): 1746-1748.
- Ma P[†], Patching SG[†], Ivanova E, Baldwin JM, Sharples D, Baldwin SA, Henderson PJ. Allantoin transport protein, Pucl, from *Bacillus subtilis*: Evolutionary relationships, amplified expression, activity and specificity. *Microbiology* 2016; 162(5): 823-836. [†]Equal contribution
- Ma P, Yuille HM, Blessie V, Göhring N, Iglói Z, Nishiguchi K, Nakayama J, Henderson PJ, Phillips-Jones MK. Expression, purification and activities of the entire family of intact membrane sensor kinases from *Enterococcus faecalis*. *Mol Membr Biol* 2008; 25(6-7): 449-473.

- Madeira F, Madhusoodanan N, Lee J, Eusebi A, Niewielska A, Tivey ARN, Lopez R, Butcher S. The EMBL-EBI Job Dispatcher sequence analysis tools framework in 2024. *Nucleic Acids Research* 2024; 52(W1): W521-W525.
- Martin JE, Giedroc DP. Functional determinants of metal ion transport and selectivity in paralogous Cation Diffusion Facilitator transporters CzcD and MntE in *Streptococcus pneumoniae*. *J Bacteriol* 2016; 198(7): 1066-1076.
- Maunder EA, Ganio K, Hayes AJ, Neville SL, Davies MR, Strugnell RA, McDevitt CA, Tan A. The role of ZntA in *Klebsiella pneumoniae* zinc homeostasis. *Microbiol Spectr* 2022; 10(1): e0177321.
- Molenda M, Kolmas J. The role of zinc in bone tissue health and regeneration - A review. *Biol Trace Elem Res* 2023; 201(12): 5640-5651.
- Palmiter RD, Huang L. Efflux and compartmentalization of zinc by members of the SLC30 family of solute carriers. *Pflugers Arch* 2004; 447(5): 744-751.
- Patzer SI, Hantke K. The ZnuABC high-affinity zinc uptake system and its regulator Zur in *Escherichia coli*. *Mol Microbiol* 1998; 28(6): 1199-1210.
- Poolman B, Knol J. Amplified expression and membrane reconstitution of transport proteins. *Biochem Soc Trans* 1999; 27(6): 912-917.
- Rahman M, Ismat F, Jiao L, Baldwin JM, Sharples DJ, Baldwin SA, Patching SG. Characterisation of the DAACS family *Escherichia coli* glutamate/aspartate-proton symporter GltP using computational, chemical, biochemical and biophysical methods. *J Membr Biol* 2017; 250(2): 145-162.
- Rahman M, Ismat F, McPherson MJ, Baldwin SA. Topology-informed strategies for the overexpression and purification of membrane proteins. *Molecular Membrane Biology* 2007; 24(5-6): 407-418.
- Rahman M, Patching SG, Ismat F, Henderson PJ, Herbert RB, Baldwin SA, McPherson MJ. Probing metal ion substrate-binding to the *E. coli* ZitB exporter in native membranes by solid state NMR. *Mol Membr Biol* 2008; 25(8): 683-690.
- Rensing C, Mitra B, Rosen BP. The *zntA* gene of *Escherichia coli* encodes a Zn(II)-translocating P-type ATPase. *Proc Natl Acad Sci U S A* 1997; 94(26): 14326-14331.
- Roberts CS, Muralidharan S, Ni F, Mitra B. Structural role of the first four transmembrane helices in ZntA, a P1B-type ATPase from *Escherichia coli*. *Biochemistry* 2020; 59(47): 4488-4498.
- Roohani N, Hurrell R, Kelishadi R, Schulin R. Zinc and its importance for human health: An integrative review. *J Res Med Sci* 2013; 18(2): 144-157.
- Routh MD, Zalucki Y, Su CC, Zhang Q, Shafer WM, Yu EW. Efflux pumps of the resistance-nodulation-division family: a perspective of their structure, function, and regulation in gram-negative bacteria. *Adv Enzymol Relat Areas Mol Biol* 2011; 77: 109-146.
- Saidijam M, Bettaney KE, Szakonyi G, Psakis G, Shibayama K, Suzuki S, Clough JL, Blessie V, Abu-Bakr A, Baumberg S, Mueller J, Hoyle CK, Palmer SL, Butaye P, Walravens K, Patching SG, O'Reilly J, Rutherford NG, Bill RM, Roper DI, Phillips-Jones MK, Henderson PJ. Active membrane transport and receptor proteins from bacteria. *Biochem Soc Trans* 2005; 33(Pt 4): 867-872.

- Saidijam M, Patching SG. Amino acid composition analysis of secondary transport proteins from *Escherichia coli* with relation to functional classification, ligand specificity and structure. *J Biomol Struct Dyn* 2015; 33(10): 2205-2220.
- Saidijam M, Psakis G, Clough JL, Meuller J, Suzuki S, Hoyle CJ, Palmer SL, Morrison SM, Pos MK, Essenberg RC, Maiden MC, Abu-bakr A, Baumberg SG, Neyfakh AA, Griffith JK, Stark MJ, Ward A, O'Reilly J, Rutherford NG, Phillips-Jones MK, Henderson PJ. Collection and characterisation of bacterial membrane proteins. *FEBS Lett* 2003; 555(1): 170-175.
- Salgueiro MJ, Zubillaga M, Lysionek A, Cremaschi G, Goldman CG, Caro R, De Paoli T, Hager A, Weill R, Boccio J. Zinc status and immune system relationship: A review. *Biol Trace Elem Res* 2000; 76(3): 193-205.
- Sambrook J, Fritsch EF, Maniatis T. *Molecular cloning: A laboratory manual*. Cold Spring Harbor Laboratory, 1989. Cold Spring Harbor, New York.
- Stark MJR. Multicopy expression vectors carrying the lac repressor gene for regulated high-level expression of genes in *Escherichia coli*. *Gene* 1987; 51: 255-267.
- Stiles LI, Ferrao K, Mehta KJ. Role of zinc in health and disease. *Clin Exp Med* 2024; 24(1): 38.
- Suryawati B. Zinc homeostasis mechanism and its role in bacterial virulence capacity. *AIP Conf Proc* 2018. 2021; 1: 070021.
- Takatani-Nakase T. Zinc transporters and the progression of breast cancers. *Biol Pharm Bull* 2018; 41(10): 1517-1522.
- Tsirigos KD, Peters C, Shu N, Käll L, Elofsson A. The TOPCONS web server for consensus prediction of membrane protein topology and signal peptides. *Nucleic Acids Res* 2015; 43(W1): W401-W407.
- Udagedara SR, La Porta DM, Spehar C, Purohit G, Hein MJA, Fatmous ME, Casas Garcia GP, Ganio K, McDevitt CA, Maher MJ. Structural and functional characterizations of the C-terminal domains of CzcD proteins. *J Inorg Biochem* 2020; 208: 111087.
- Valencia EY, Braz VS, Guzzo C, Marques MV. Two RND proteins involved in heavy metal efflux in *Caulobacter crescentus* belong to separate clusters within proteobacteria. *BMC Microbiol* 2013; 13: 79.
- Wang D, Hosteen O, Fierke CA. ZntR-mediated transcription of *zntA* responds to nanomolar intracellular free zinc. *J Inorg Biochem* 2012; 111: 173-181.
- Ward A, O'Reilly J, Rutherford NG, Ferguson SM, Hoyle CK, Palmer SL, Clough JL, Venter H, Xie H, Litherland GJ, Martin GE, Wood JM, Roberts PE, Groves MA, Liang WJ, Steel A, McKeown BJ, Henderson PJ. Expression of prokaryotic membrane transport proteins in *Escherichia coli*. *Biochem Soc Trans.* 1999; 27(6): 893-899.
- Ward A, Sanderson NM, O'Reilly J, Rutherford NG, Poolman B, Henderson PJF. The amplified expression, identification, purification, assay and properties of hexahistidine tagged bacterial membrane transport proteins. In: Baldwin SA (Ed) *Membrane transport – a Practical Approach*, 2000. Oxford:Blackwell, pp. 141-166.

- Wei Y, Fu D. Binding and transport of metal ions at the dimer interface of the *Escherichia coli* metal transporter YiiP. *J Biol Chem* 2006; 281(33): 23492-23502.
- Without B, Boekhout M, Brock M, Kingma J, Heerikhuizen HV, Leij LD. An efficient and reproducible procedure for the formation of spheroplasts from variously grown *Escherichia coli*. *Anal Biochem* 1976; 74(1): 160-170.
- Xu Y, Xiao G, Liu L, Lang M. Zinc transporters in Alzheimer's disease. *Mol Brain* 2019; 12(1): 106.
- Xue J, Xie T, Zeng W, Jiang Y, Bai XC. Cryo-EM structures of human ZnT8 in both outward- and inward-facing conformations. *eLife* 2020; 9: e58823.
- Yi B, Huang G, Zhou Z. Different role of zinc transporter 8 between type 1 diabetes mellitus and type 2 diabetes mellitus. *J Diabetes Investig* 2016; 7(4): 459-465.
- Yin S, Duan M, Fang B, Zhao G, Leng X, Zhang T. Zinc homeostasis and regulation: Zinc transmembrane transport through transporters. *Crit Rev Food Sci Nutr* 2023; 63(25): 7627-7637.
- Zhang S, Fu C, Luo Y, Xie Q, Xu T, Sun Z, Su Z, Zhou X. Cryo-EM structure of a eukaryotic zinc transporter at a low pH suggests its Zn²⁺-releasing mechanism. *J Struct Biol* 2023; 215: 107926.
- Zheng C, Zhai Y, Qiu J, Wang M, Xu Z, Chen X, Zhou X, Jiao X. ZntA maintains zinc and cadmium homeostasis and promotes oxidative stress resistance and virulence in *Vibrio parahaemolyticus*. *Gut Microbes* 2024; 16(1): 2327377.